SCIENTIFIC REPORTS

OPEN

SUBJECT AREAS:
METAMATERIALS
NANOPHOTONICS AND PLASMONICS

Received
27 May 2014

Accepted
22 August 2014

Published
11 September 2014

Correspondence and requests for materials should be addressed to K.V.S. (sxk923@case.edu) or G.S. (giuseppe.strangi@case.edu)

Large spontaneous emission rate enhancement in grating coupled hyperbolic metamaterials

Kandammathe Valiyaveedu Sreekanth[1], Koduru Hari Krishna[2], Antonio De Luca[2] & Giuseppe Strangi[1,2]

[1]Department of Physics, Case Western Reserve University, 10600 Euclid Avenue, Cleveland, Ohio. 44106-7079, USA, [2]Department of Physics and CNR-IPCF UOS di Cosenza, University of Calabria, 87036 - Rende (Italy).

Hyperbolic metamaterial (HMM), a sub-wavelength periodic artificial structure with hyperbolic dispersion, can enhance the spontaneous emission of quantum emitters. Here, we demonstrate the large spontaneous emission rate enhancement of an organic dye placed in a grating coupled hyperbolic metamaterial (GCHMM). A two-dimensional (2D) silver diffraction grating coupled with an Ag/Al_2O_3 HMM shows 18-fold spontaneous emission decay rate enhancement of dye molecules with respect to the same HMM without grating. The experimental results are compared with analytical models and numerical simulations, which confirm that the observed enhancement of GCHMM is due to the outcoupling of non-radiative plasmonic modes as well as strong plasmon-exciton coupling in HMM via diffracting grating.

In view of cutting-edge scientific advances in the field of nanophotonics, unique multi-scale metamaterials have been recognized as versatile engineered structures to mitigate classical limitations of optics and enable numerous challenging applications. The main core in all metamaterials comprises of fabricating a medium composed of unit cells of size far below the excitation wavelength. In contrast to existing optical metamaterials in the visible and near-infrared wavelength regions, hyperbolic metamaterials (HMMs) are distinguished as promising class of metamaterials owing to their characteristic features like hyperbolic form of the iso-frequency dispersion curve and the directional nature of light propagation[1–4]. The artificial HMMs can be analogous to uniaxial metacrystals with an extremely anisotropic dielectric tensor, $\varepsilon = \mathrm{diag}\,[\varepsilon_{xx}, \varepsilon_{yy}, \varepsilon_{zz}]$ such that $\varepsilon_{xx} = \varepsilon_{yy}$ and $\varepsilon_{zz} \cdot \varepsilon_{xx} < 0$, which leads to a hyperbolic dispersion exhibiting dielectric properties ($\varepsilon > 0$) in one direction and metallic nature in another direction ($\varepsilon < 0$). This distinctive physical consequence of dispersion relation enables the propagation of waves with very high wavevectors, known as high-k waves, showing a broadband singularity in the density of photonic states[5]. These interesting properties of HMMs promise a large variety of substantial futuristic applications such as spontaneous emission enhancement[5–10], nanoimaging[11–13], negative refraction[14–16], super-planckian thermal emission[17], biosensing[18] and Dyakonov plasmonics[19]. The hyperbolic dispersion of HMMs leads to the existence of high photonic density of states, which can be investigated by understanding the modifications in spontaneous emission of emitters placed in the vicinity of HMM[5].

In cavity quantum electrodynamics, closed cavities (microcavities) and open cavities (photonics crystals) have been employed as significant tools to understand cavity quantum electrodynamics and hence for the study of modification of spontaneous emission enhancement by the Purcell effect[20–22]. However, the incapability for 'microcavities' and 'photonic crystal' systems to obtain high quality factor resonance make them unviable for Purcell enhancement. This incompatibility of cavity technologies pushed towards the discovery of novel systems whose exhibit broadband Purcell effect. Hyperbolic metamaterials are promising and reliable systems in comparison to conventional cavity approaches due to the existence of a large number of electromagnetic states, which lead to a divergence in the photonic density of states allowing a broadband control. In particular, HMMs play a vital role to confine the power emitted by emitters in large spatial wavevector channels. This will open new routes for innovative photonic device applications from broadband single photon sources to strong coupling of emitters and plasmonics. In past years, many research groups have explored about modifications in the spontaneous emission rates of organic dyes and quantum dots positioned in the close vicinity of the surface of a metamaterial with hyperbolic dispersion[5–7]. However, the Purcell enhancement of HMM is limited at the far-field due to the non-radiative behaviour of plasmonic modes in HMM. Recently, nanopatterned hyperbolic metamaterials have been proposed for outcoupling the non-radiative plasmonic modes and to enhance the spontaneous emission

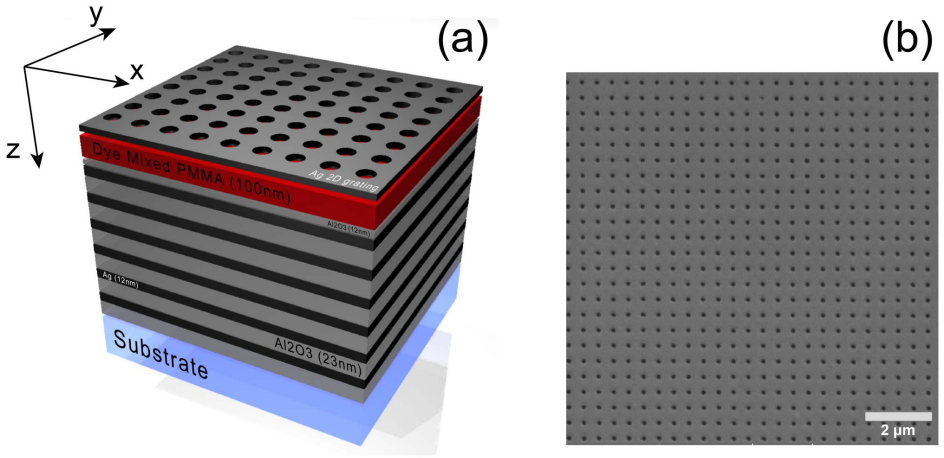

Figure 1 | Fabrication of GCHMM (a) Schematic of fabricated Ag diffraction grating coupled Ag/Al_2O_3 HMM (GCHMM), which consists of 6 pairs of Ag/Al_2O_3. (b) SEM image of 2D Ag diffraction grating on top of the PMMA layer with an average period of 500 nm and hole size of 160 nm.

rates of fluorescent molecules[23,24]. Here we propose another novel approach, which is based on a grating coupled HMM (GCHMM) configuration to further improve the spontaneous emission rate of emitters placed nearby HMM, by exploiting the unique property of a hypergrating to outcouple and extract the non-radiative plasmonic modes. We have recently demonstrated that a grating coupled HMM geometry (hypergrating geometry) can be used to excite both surface and bulk plasmon modes from a HMM system[25]. In the present work, we experimentally and numerically investigate the large spontaneous emission rate enhancement of fluorescent molecules using a GCHMM configuration.

Results

Design and fabrication of GCHMM. The designed grating coupled HMM (GCHMM) structure (Fig. 1 (a)) is fabricated by following sequential depositions of 12 alternated layers of alumina (Al_2O_3) and silver (Ag) thin films by using conventional electron beam and thermal evaporation techniques, respectively. All the thin films are grown over micro-glass substrates and Al_2O_3, Ag pellets are used as source materials. Spectroscopic ellipsometry measurements have been carried out to estimate the thicknesses of grown thin films. The measured thickness of Al_2O_3 and Ag are 23 nm and 12 nm, respectively. Therefore, in the present investigation evaluated fill fraction of Ag is 34%. To investigate the influence of designed HMM on spontaneous emission enhancement a dye doped PMMA layer (thickness around 100 nm) is spin coated over a pre-deposited Al_2O_3 spacer (12 nm) on the HMM structure (see Fig. 1(a)). In this process, an organic dye (Coumarin 500) is initially dissolved in ethanol (0.3% by wt.) solution and in the next step resultant solution is dissolved in PMMA resist. For comparative analysis, a reference sample is fabricated by spin coating a layer of dye-doped PMMA over a pre-deposited Al_2O_3 spacer (same thickness of 12 nm) over glass substrates. The dielectric constants of thin films of Ag and Al_2O_3 are experimentally determined using spectroscopic ellipsometry. The real (red line) and imaginary (blue line) permittivity values of Ag as well as dielectric constants (black line) of Al_2O_3 are shown in Fig. 2 (a). One can clearly see that real permittivity values of Ag show a well-known decreasing trend towards strongly negative values. This is due to the Drude-type response of free electrons in metals at higher wavelengths[26]. In the fabricated HMM structure, the individual metal and dielectric layers dimensions are satisfying the criteria of effective medium theory (EMT) to achieve homogeneity. Therefore the uniaxial dielectric tensor components of an anisotropic medium of HMM are evaluated using EMT[27]. In the calculation, the optical constants of Ag and Al_2O_3 are taken from experimentally obtained values (Fig. 2(a)). The evaluated dielectric permittivity tensor components of the fabricated HMM (i.e $\varepsilon_{ll}(\varepsilon_x = \varepsilon_y) < 0$ and $\varepsilon_{\perp}(\varepsilon_z) > 0$) imply a hyperbolic dispersion above the wavelength of 430 nm, at which

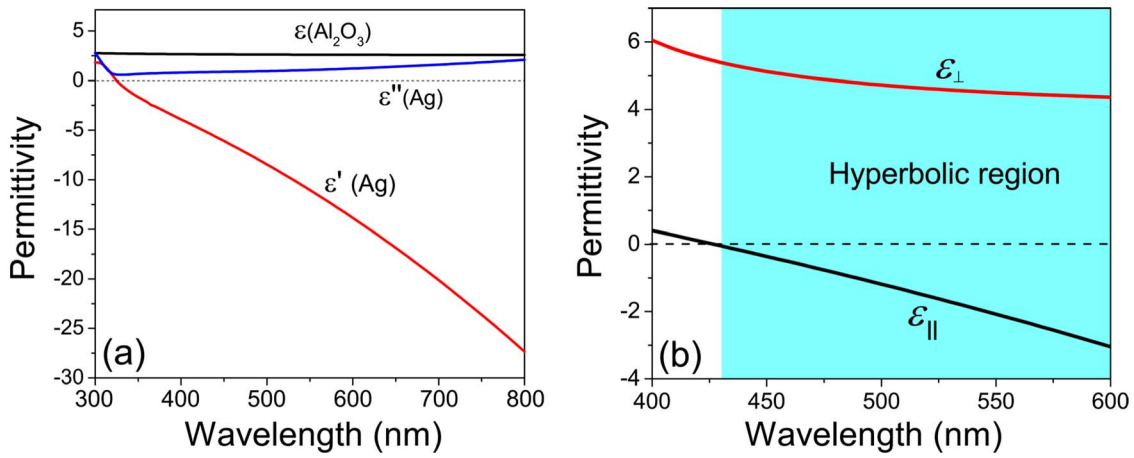

Figure 2 | Characterization of GCHMM: (a) Experimentally determined permittivity values of Ag and Al_2O_3 thin films. The red and blue lines represent the real and imaginary permittivity values of Ag, respectively and black line represents the permittivity values of Al_2O_3. (b) Real parts of effective permittivity of Ag/Al_2O_3 HMM determined with effective media theory. The Ag/Al_2O_3 HMM shows hyperbolic dispersion at $\lambda \geq 430$ nm.

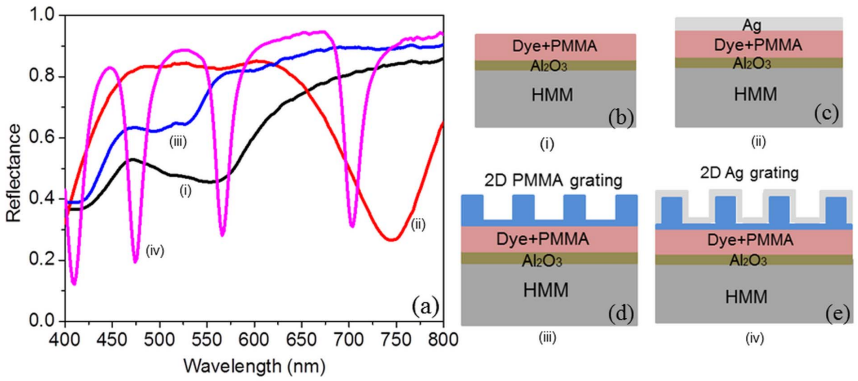

Figure 3 | Reflectance spectra as a function of excitation wavelength: (a) Reflectance spectrum of various samples obtained at incident grazing angle of 50°. The studied samples are shown in Figs. (b) to (e). The GCHMM sample (iv) shows four prominent reflectance dips corresponding to the excited plasmonic modes (both surface and bulk plasmon polaritons) from the geometry.

transition occurs from elliptical to hyperbolic dispersion as shown in Fig. 2(b).

A grating coupling technique is used to excite plasmonic modes associated with HMM. By following the electron-beam lithographic technique, a 2D diffraction grating is patterned above the dye mixed PMMA layer over the HMM, followed by deposition of an Ag layer of thickness 20 nm. The fabricated grating has an average period of 500 nm and average hole diameter of 160 nm. The total area of patterned grating structure over HMM is around 5 mm × 5 mm. The SEM image of patterned 2D Ag diffraction grating is shown in Fig. 1(b). During the diffraction grating fabrication, Ag film of thickness 20 nm is directly deposited on the PMMA diffraction grating, but not directly on the dye mixed PMMA layer. Note that a thin PMMA spacer layer is at the interface between Ag film and dye mixed PMMA layer because a thin layer of PMMA resist always left during the resist development (etching) process (see Fig. 3 (e)). Hence this thin spacer layer can avoid the nonradiative contribution due to quenching at the Ag-Dye mixed PMMA interface. According to grating coupling principle, the surface plasmon modes can be excited when the wavevector of the grating diffraction orders are greater than the incident light. Under this condition, diffraction orders are no longer propagating waves, but evanescent field, and the enhanced wavevector of evanescent field is responsible for the coupling of incident light to surface plasmon modes by following the condition $k_{SPP} = n_0 k_0 \sin\theta \pm mk_{gx} \pm nk_{gy}$. Being θ the incident grazing angle, n_0 is the refractive index of incident medium, $k_0 = 2\pi/\lambda$ is the vacuum wavevector, m and n are the grating diffraction orders and $k_g = 2\pi/\Lambda$ is the grating wavevector with Λ being the grating period. On the other hand, by introducing a diffraction grating on top of the HMM, it is possible to diffract light and produce a wide range of wave vectors into the HMM. Due to the existence of impedance mismatch at the various openings, the generated wave vectors can couple through the surface modes[28]. It should be noted that the large thickness (around 100 nm) of dye dissolved PMMA layer can decrease the coupling efficiency of the proposed structure. Nonetheless, unintentional scatterers are common in dye dissolved PMMA layer and these scatterers also enable the excitation of surface plasmon modes through the coupling of incident light to the surface plasmon polaritons (SPPs)[29,30]. These two phenomena contribute to the excitation of high-k modes inside the HMM. Since the emitter is placed inside the GCHMM, it is a challenging operation to couple the incident radiation to the emitter because of the impedance mismatch between air and HMM. However, the grating coupling helps to outcouple the highly confined modes from the structure to the far field. In order to show the excited plasmonic modes from HMM, the reflectance spectrum of different samples for p-polarization is obtained and shown in Fig. 3 (a) (also see Supplementary Fig. 1 & Fig. 2). Here incident grazing angle is set to be 50°. One can observe that 2D Ag grating coupled HMM supports four narrow reflectance minima that correspond to expected plasmonic modes (both surface and bulk plasmon modes). The reflectance spectrum of GCHMM is simulated using scattering matrix method (SMM)[31,32] that is shown in Fig. S3 (Supplementary Fig. 3). A good agreement with experimental result is obtained. In addition, Ag film deposited HMM shows a broad reflectance minimum at higher wavelength (750 nm), which is due to the presence of Ag scatterers intermixed at the interface with dye doped PMMA layer as experimentally verified (see Supplementary Fig. 4).

Experimental results. Time-resolved photoluminescence measurements are performed to study the decay rate of various samples. An ultrafast optical setup has been used (see Supplementary Fig. 5); it consists of a Ti: Sapphire tunable femtosecond laser, a Pulse Picker, a Second Harmonic Generator and a spectrofluorometer used for time-correlated single photon counting (TCSPC) measurements. The time resolution of the TCSPC instrument is ≤5 ps. The Coumarin molecules are excited by using a pulsed laser at 380 nm with a pulse width of about 120 fs and a repetition rate of 4 MHz. The maximum emission wavelength of Coumarin 500 dye dissolved PMMA is observed at 470 nm for 380 nm excitation wavelength (see Supplementary Fig. 6). In order to show the transition from elliptical to hyperbolic dispersion, the investigated emission wavelengths are varied. The short-living excitonic states of the emitters placed in the vicinity of the HMM and the measured fluorescent lifetime as a function of emission wavelength, would represent a clear signature of the transition from elliptical to hyperbolic dispersion. The fluorescence time decay curves of four samples at spectral regions such as elliptical dispersion (420 nm), the critical wavelength (430 nm), and the hyperbolic dispersion (450 nm) are shown in Fig. 4. Four different samples such as reference (pink curve), HMM (red curve), Ag film deposited HMM (black curve) and GCHMM (blue curve) are investigated for comparison. It was not possible to fit the decay rate of all four samples using a single exponential function because the detected signals arise from the collective response of molecules randomly distributed in PMMA[23]. Therefore the data have been fitted using three exponential functions, $R(t) = B_1 e^{-t/\tau_1} + B_2 e^{-t/\tau_2} + B_3 e^{-t/\tau_3}$ with τ_i being the decay times. Since longer time (τ_3) is attributed to uncoupled dye molecules, located above the coupling distance from the HMM, we use shorter decay times (τ_1 and τ_2) to predict the decay rate enhancement, since shorter decay times are related to molecules strongly coupled with HMM[23]. The transition from elliptical to hyperbolic dispersion is evident from the obtained curves, showing a large variation in time decay for HMM compared to reference sample when the emission wavelength is varied from elliptical to hyperbolic region (also see Supplementary Fig. 7 & Fig. 8). The

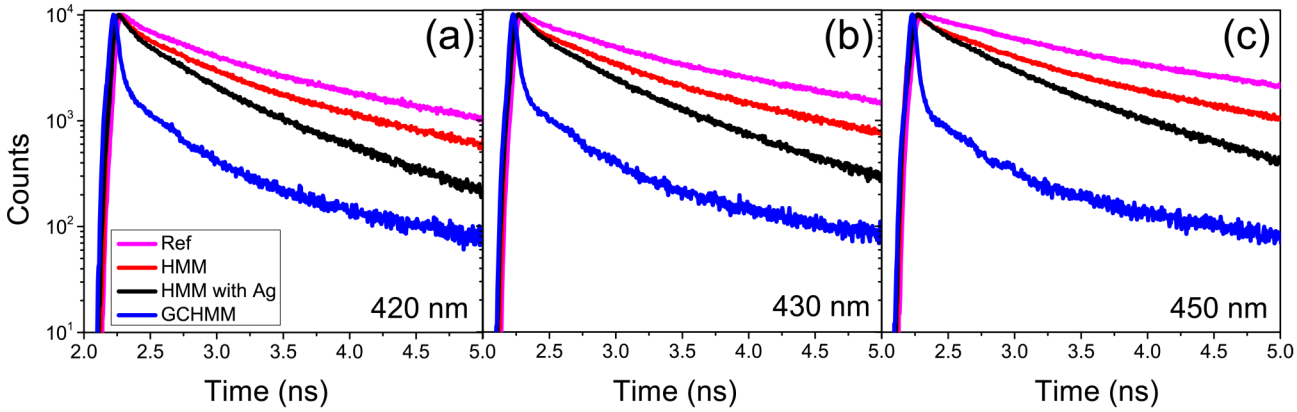

Figure 4 | Time-resolved photoluminescence measurements of Coumarin dye on various samples, Ref (pink), HMM (red), HMM with Ag (black), and GCHMM (blue)) with emission wavelength: (a) in elliptical region (λ_e = 420 nm), (b) at critical wavelength (λ_c = 430 nm), and (c) in hyperbolic region (λ_e = 450 nm).

coupling of the high-k metamaterial states is responsible for the observed behaviour of HMM[5]. The observed response of HMM definitely supports the existence of high k-modes in the fabricated Ag/Al_2O_3 HMM. However, the observed results are not in good agreement with previously reported results[5]. This could be due to the low internal quantum yield of the Coumarin 500 dye in PMMA, broadband dye emission spectrum and higher metallic fill fraction. The decay rate enhancement is defined as the inverse of decay time.

To verify the large decay rate enhancement of proposed configuration, the GCHMM sample is compared with HMM and Ag film deposited HMM samples. Throughout the wavelength spectral range of the HMM, one can see that the GCHMM (blue curve) shows a large decay rate variation with respect to HMM (red curve) and Ag film deposited HMM (black curve). In addition, the decay rate variation increases when the emission wavelength is varied from the elliptical to hyperbolic spectral region of the HMM. The maximum decay rate is obtained for GCHMM for all wavelengths, which are 1/0.035 ns^{-1}, 1/0.030 ns^{-1}, and 1/0.031 ns^{-1} for 420 nm, 480 nm and 510 nm, respectively. The corresponding decay rates at the respective wavelengths are 1/0.220 ns^{-1}, 1/0.491 ns^{-1}, and 1/0.575 ns^{-1} for HMM and 1/0.071 ns^{-1}, 1/0.353 ns^{-1} and 1/0.534 ns^{-1} for Ag film deposited HMM. Note that the first decay time (τ_1) is considered here for comparison. This large decay rate of GCHMM is attributed to the strong coupling of emitters to HMM via metallic diffraction grating. Specifically, the metallic grating excites the plasmonic Bloch modes (high-k modes) as well as surface plasmon polaritons of HMM and there is a strong overlap between these modes with the quantum emitters, which leads to a broadband enhancement of photonic density of states (PDOS). In addition, 2D diffraction grating scatters the high-k modes of HMM into well-defined free space modes. The sub-wavelength confinement of the emitter inside the GCHMM structure also enhances the decay rate. Furthermore, improved decay rate is observed for Ag film deposited HMM at certain emission wavelengths as compared to HMM. It is attributed to the presence of Ag scatterers intermixed at the interface with dye doped PMMA layer and nonradiative contribution due to quenching at the Ag-dye doped PMMA interface.

In order to emphasize the improved plasmon-exciton coupling in GCHMM, normalized lifetimes of GCHMM and Ag film deposited HMM are compared (the fitting curves are shown in Supplementary Fig. 9). The first (τ_1) and second (τ_2) decay times of both samples, normalized with respect to HMM as a function of emission wavelength, are shown in Fig. 5(a) and Fig. 5(b), respectively. It is evident from those figures that same decay rate variation is obtained for both decay times. For GCHMM, lifetime values are higher in elliptical region and smaller in hyperbolic region. This behaviour represents the preferential emission of high-k modes from GCHMM. However, the lifetimes of Ag film deposited HMM are randomly varying along the spectral range showing that the presence of Ag film does not support the preferential emission of high-k modes. The smaller life-

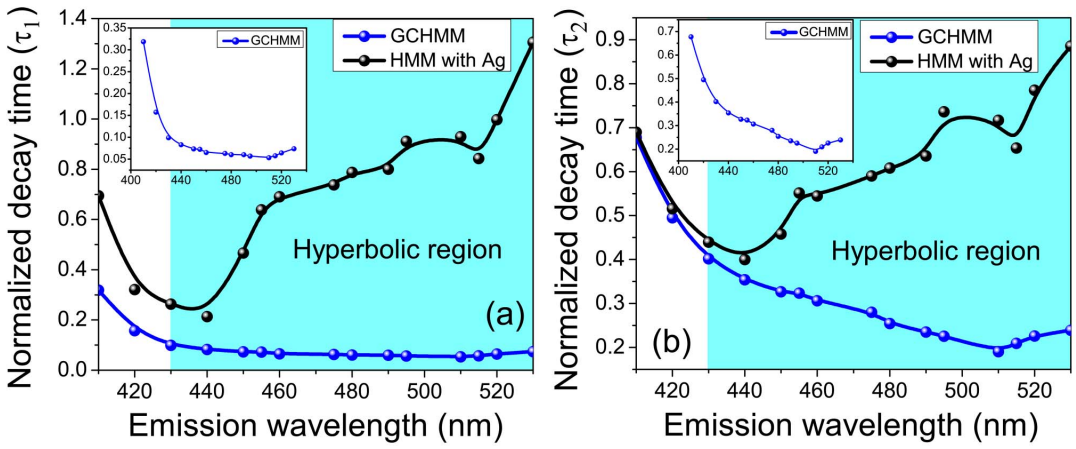

Figure 5 | Lifetimes of dye on GCHMM and Ag film deposited HMM normalized with respect to HMM sample: for (a) first decay time (τ_1) and (b) second decay time (τ_2). The solid lines are for eye guide. Enlarged plot of normalized decay time of GCHMM is shown in the inset of (a) and (b). Normalized lifetime is studied as a function of emission wavelength from elliptical to hyperbolic dispersion. In the case of GCHMM, a maximum decay rate is observed at 510 nm for both decay times.

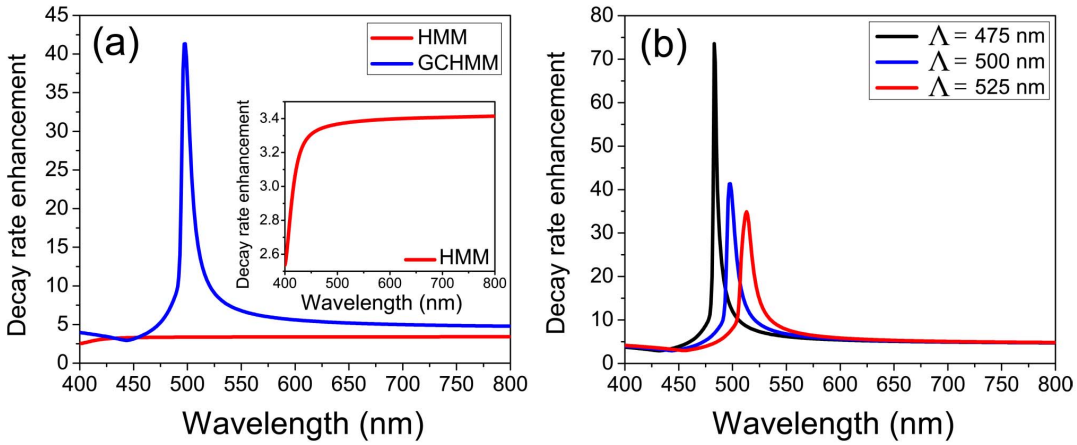

Figure 6 | Numerical simulation results (a) Calculated decay rate enhancement of HMM and GCHMM with period 500 nm. Enlarged plot of decay rate enhancement of HMM is shown in the inset of (a). (b) Tuning of decay rate enhancement of GCHMM with grating period.

time values of GCHMM in hyperbolic region are due to the hyperbolic dispersion. It should be noted that the lifetime values of GCHMM behave non-monotonically as function of the wavelength, they decrease by reaching a minimum value at 510 nm, then in the same hyperbolic region show a change of slope towards higher lifetime values. The observed behaviour is a clear signature of the outcoupling ability of GCHMM. According to τ_1, a maximum of 18-fold decay rate enhancement is obtained for GCHMM at 510 nm emission wavelength, whereas 5-fold decay rate enhancement is obtained for τ_2. In comparison to Ag film deposited HMM, the maximum decay rate enhancement for GCHMM is observed at 510 nm, which is around 17 times and 4 times higher for τ_1 and τ_2, respectively. The observed large spontaneous emission rate enhancement of GCHMM is mainly due to radiative recombination rate, whereas non-radiative recombination rate is negligible in GCHMM. Thus the observed behaviour of GCHMM strongly supports the influence of diffraction grating on the spontaneous emission rate enhancement. The main advantage of GCHMM compared to the other two samples is the ability to outcouple the high wavevector plasmonic modes from HMM to far-field, by the detection of fast-decaying signals from emitters strongly coupled to the multilayer structure[23]. In the case of HMM, the field inside the multilayer is highly confined and it is unable to be detected at far field due to the evanescent nature of field at the top surface of HMM. However, the grating coupler helps to translate the evanescent field to a propagating field for far-field detection. This is evident from the time-resolved photoluminescence measurements.

Simulation results. A numerical simulation has been implemented to obtain a complete analysis of the enhanced emission rates observed in the experimental section. In order to study the decay rate enhancement analytically, we use a semiclassical approach in which quantum emitters have been considered as radiating point dipoles[33]. According to this method, the decay rate enhancement with respect to vacuum of a point dipole with dipole moment 'μ', placed at a distance 'd' from a HMM is given by[2,5,8],

$$\beta = \frac{\Gamma}{\Gamma_0} = (1-\eta) + \frac{3\eta}{2k_0^3}\,\mathrm{Re}\int_0^\infty \exp(2ik_z d)\frac{k_{ll}\,dk}{k_z|\mu^2|}$$
$$\left\{\frac{1}{2}\mu_{ll}^2[(1+r_s)k_0^2-(1-r_p)k_z^2]+\mu_\perp^2(1+r_p)k_{ll}^2\right\}$$

Where η is the intrinsic quantum yield of the emitter, k_0 is the wavevector of the medium where the emitter resides, k_{ll} is the wavevector parallel to interface of the HMM, $k_z = \sqrt{k_0^2 - k_{ll}^2}$ and r_s, r_p are the Fresnel reflection coefficients for s- and p-polarization, respectively. Here the Fresnel reflection coefficients of the HMM are obtained with transfer matrix method[34]. In our simulation, the relative permittivity of Ag is obtained from Drude model, $\varepsilon_{Ag}(\omega) = 1 - \left(\omega_p^2/(\omega^2 + i\nu\omega)\right)$ with $\omega_p = 11.5\ fs^{-1}$ and $\nu = 0.083\ fs^{-1}$ [35]. Note that the point dipole (emitter) resides in PMMA and refractive index of PMMA is set to be 1.49 for wavelengths in the range of 400–800 nm[36]. Here the separation distance and intrinsic quantum yield of Coumarin dye is taken as 12 nm and 0.98[37], respectively.

Figure 6 shows the decay rate enhancement of HMM and GCHMM. As shown in the inset of Fig. 6 (a), an improved decay rate enhancement is observed for HMM in the hyperbolic spectral region (above 430 nm). Due to the strong coupling between the emitter and the high-k modes in HMM, the decay rate enhancement monotonically increases in hyperbolic region. In particular, this coupling strength increases for shorter interaction distances (d/λ). In comparison to HMM, GCHMM shows improved decay rate enhancement for all wavelengths. However, for a particular wavelength band, GCHMM provides very large enhancement of β with respect to HMM. For 500 nm grating period, the maximum β is obtained at 497 nm wavelength that is 12 times higher than HMM. It shows that the simulation results are in good agreement with experiments. However, there is a slight discrepancy in wavelength at which maximum emission rate is observed. This can be attributed to the non-uniform periodicity (average period = 500 nm) of fabricated diffraction grating as compared to uniform periodicity (500 nm) considered in the simulation. According to the simulation model, the maximum value of β in GCHMM depends on the periodicity of the diffraction grating. Note that the periodicity of the grating is introduced in the calculation of Fresnel reflection coefficients for s- and p-polarization, i. e, $k_x = n_0 k_0 \sin\theta \pm m(2\pi/\Lambda_x) \pm n(2\pi/\Lambda_y)$ with $\Lambda_x = \Lambda_y = \Lambda$ for grating with square lattice symmetry. The decay rate enhancement of GCHMM with different grating periods is shown in Fig. 6(b). It shows the possibility of tuning the spectral position of the maximum β and broadband enhancement of β by varying the grating period. According to Fig. 6(b), the larger enhancement of β is observed for smaller period (Λ = 475 nm) that is due to the fact that smaller periods provide better momentum match and outcouple most of the high-k modes from HMM[23]. Since HMM provides broadband decay rate enhancement in hyperbolic region, a single period diffraction grating can outcouple a single wavelength as observed in our simulation. However, up on designing a proper chirped grating a broadband outcoupling of plasmonic modes is possible[38,39]. Therefore the broadband outcoupling of single

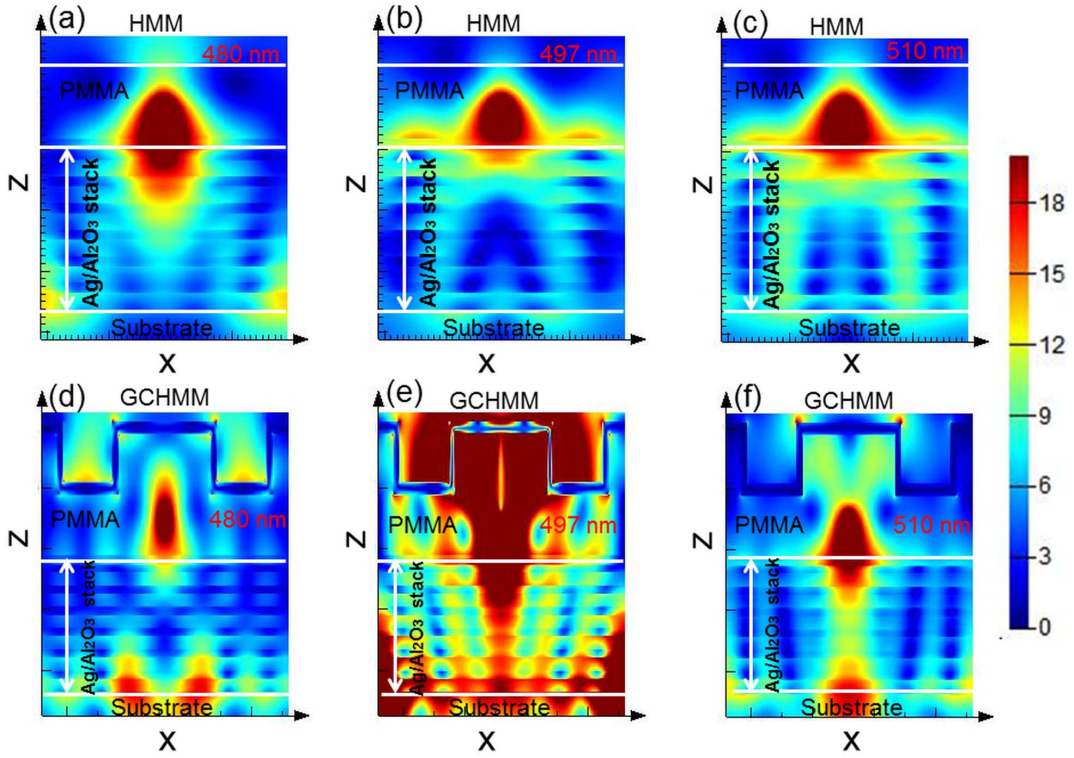

Figure 7 | FDTD simulation results for HMM and GCHMM. Cross-sectional map of the electric field distribution in the hyperbolic region with emission wavelength such as 480 nm, 497 nm, and 510 nm: (a)–(c) for HMM and (d)–(f) for GCHMM. For GCHMM, the period of the grating is set to be 500 nm.

photon as well as outcoupling of greater number of high-k modes can be achieved by engineering a modified diffraction grating geometry.

We further performed finite difference time domain (FDTD) numerical simulation to show the effect of grating coupling in GCHMM. In order to compare the obtained results, the electromagnetic field distribution along the HMM and GCHMM is simulated by assuming that the quantum emitter (point dipole) with a specified emission wavelength resides in PMMA above the multilayer. In hyperbolic region, the electric field (EF) cross-sectional map (xz-plane) of both HMM and GCHMM as a function of emission wavelength is shown in Fig. 7. According to Fig. 7(a) to 7(c), the magnitude of EF for HMM increases when the emission wavelength is varied from 480 to 510 nm. This is due to the monotonic increase of the fluorescence decay rate of HMM in the hyperbolic region. In comparison to HMM, GCHMM provides enhanced EF on the substrate as well as above the grating (in air), which evidently shows the outcoupling effect of GCHMM. It is clearly visible that the EF distribution on GCHMM extensively varies with emission wavelength. The maximum EF distribution for GCHMM along the multilayer and the strong coupling between grating, and point dipole is observed for 497 nm emission wavelength. This behaviour of GCHMM definitely supports the maximum decay rate enhancement observed at 497 nm in Fig. 6(a). Note that the enhanced EF distribution is observed close to the surface of the HMM in which higher plasmonic density of states can be outcoupled. In the case of GCHMM, the enhanced field distribution observed at 497 nm definitely supports a strong overlap between the excited high-k modes and quantum emitter, which can provide a broadband enhancement of photonic density of states, in addition to an outcoupling effect from GCHMM. As mentioned before, the outcoupling strength depends on the periodicity and the geometry of the diffraction grating. In short, the outcoupling of non-radiative plasmonic modes as well as strong plasmon-exciton coupling through the diffraction grating is responsible for the observed large spontaneous emission decay rate enhancement in GCHMM.

Discussion

In summary, we designed and fabricated a grating coupled hyperbolic metamaterial based on Ag/Al_2O_3 multilayers to show the outcoupling effect and large spontaneous emission rate enhancement of fluorescent molecules. In comparison to Ag/Al_2O_3 HMM without diffraction grating, we obtained 18-fold spontaneous emission rate enhancement of dye molecules placed in the close proximity of GCHMM. Then we performed simulation based on a semiclassical approach to show the decay rate enhancement analytically. We further carried out FDTD numerical simulation to show the enhanced field distribution and outcoupling effect in GCHMM. A good agreement with experiment and simulation is obtained, which confirms that the observed enhancement of GCHMM is due to the outcoupling of non-radiative plasmonic modes as well as strong plasmon-exciton coupling in HMM via diffracting grating. The proposed grating coupled configuration can offer the possibility of engineering the plasmonic density of states for Purcell factor enhancement for potential applications including biosensing[40], surface-enhanced Raman spectroscopy[41] and single photon sources[21].

Methods

Sample fabrication and characterization. Hyperbolic metamaterials were realized by sequential deposition of Al_2O_3 and Ag layers on a glass substrate (Micro slides from Corning) using E-beam evaporation of Al_2O_3 pellets (from Kurt J. Lesker Company) and thermal evaporation of Ag pellets (from Kurt J. Lesker Company), respectively. The deposition rate of both materials are set to be 0.3 A/s. Coumarin 500 dye (from Exciton) was initially dissolved in ethanol (0.3% by wt. in ethanol solution) and then the solution was dissolved in PMMA resist (950PMMA C2 Resist from MICROCHEM). As prepared solution was spin coated on the HMM sample at 5000 rpm, in order to get a thickness of around 100 nm. The thickness was measured using a Stylus Profilometer (KLA-Tencor P-6). Two-dimensional diffraction grating on top of the dye dissolved PMMA was fabricated using Electron-beam lithography

(Tescan Vega). Initially, MMA resist (8.5 MMA EL 11 from MICROCHEM) was spin coated on the sample at 4000 rpm and baked at 180°C for 2 min. After some time, PMMA resist (950PMMA C2 Resist from MICROCHEM) was spin coated at 5000 rpm and baked at 180°C for 3 min. As prepared sample was patterned using e-beam lithography with dosage 200 μC/cm^2 and beam intensity 8. The exposed samples were developed using MIBK: IPA solution for 90 s and IPA for 30 s. The developed samples were imaged using scanning electron microscope (SEM by Tescan Vega), confirming that the periodic holes were exactly fitting the design. After that an Ag layer of 20 nm thickness was deposited directly on top of the sample using thermal evaporation of Ag pellets (from Kurt J. Lesker Company). As prepared samples were again imaged using SEM to see the uniformity of Ag layer on the gratings. Variable Angle Spectroscopic Ellipsometry (J. A. Woollam Co., Inc, V-VASE) was used to obtain the thicknesses and optical constants of Ag and Al_2O_3 thin films. The reflectivity spectra as a function of incident angle and excitation wavelengths were acquired using a J.A. Woollam Co. Inc V-VASE instrument with an angular resolution of 1° and wavelength spectroscopic resolution of 1 nm. The transmission measurements were performed using both J.A. Woollam Co. Inc V-VASE instrument and UV-Vis Spectrophotometer (Cary Series).

Numerical simulations. The decay rate enhancement was numerically computed with Matlab. The outcoupling property of diffraction grating is introduced in the Fresnel reflection coefficients calculation, where the wavevector of the incident beam is taken as $k_x = n_0 k_0 \sin\theta \pm m(2\pi/\Lambda_x) \pm n(2\pi/\Lambda_y)$ with $\Lambda_x = \Lambda_y = \Lambda$ for grating with square lattice symmetry. Here we assumed that $+m$ and $+n$ diffraction orders are responsible for modes excitation. However, commercially available lumerical FDTD software was used to simulate the electric field distribution. In the numerical simulation, the periodic boundary condition with smallest spatial grid size of 1 nm is used for the iteration to maintain the accuracy and stability of the FDTD simulation.

1. Poddubny, A., Iorsh, I., Belov, P. & Kivshar, Y. Hyperbolic metamaterials. *Nat. Photon.* **7**, 948–957 (2013).
2. Cortes, C. L., Newman, W., Molesky, S. & Jacob, Z. Quantum nanophotonics using hyperbolic metamaterials. *J. Opt.* **14**, 063001 (2012).
3. Pendry, J. B. A Chiral route to negative refraction. *Science* **306**, 1353–1355 (2004).
4. Smith, D. R., Padilla, W. J., Vier, D. C., Nemat-Nasser, S. C. & Shultz, S. Composite medium with simultaneously negative permeability and permittivity. *Phys. Rev. Lett.* **84**, 4184 (200).
5. Krishnamoorthy, H. N. S., Jacob, Z., Narimanov, E., Kretzschmar, I. & Menon, V. M. Topological transitions in metamaterials. *Science* **336**, 205–209 (2012).
6. Jacob, Z. *et al.* Engineering photonic density of states using metamaterials. *Appl. Phys. B* **100**, 215–218 (2012).
7. Jacob, Z., Smolyaninov, I. I. & Narimanov, E. E. Broadband Purcell effect: Radiative decay engineering with metamaterials. *Appl. Phys. Lett.* **100**, 181105 (2012).
8. Newman, W. D., Cortes, C. L. & Jacob, Z. Enhanced and directional single-photon emission in hyperbolic metamaterials. *J. Opt. Soc. Am. B* **30**, 766–775 (2013).
9. Noginov, M. A. *et al.* Controlling spontaneous emission with metamaterials. *Opt. Lett.* **35**, 1863 (2010).
10. Sreekanth, K. V., Biaglow, T. & Strangi, G. Directional spontaneous emission enhancement in hyperbolic metamaterials. *J. Appl. Phys.* **114**, 134306 (2013).
11. Ono, A., Kato, J.-I. & Kawata, S. Subwavelength optical imaging through a metallic nanorod array. *Phys. Rev. Lett.* **95**, 267407 (2005).
12. Salandrino, A. & Engheta, N. Far-field subdiffraction optical microscopy using metamaterial crystals: Theory and simulations. *Phys. Rev. B.* **74**, 075103 (2006).
13. Liu, Z., Lee, H., Xiong, Y., Sun, C. & Zhang, X. Far-field optical hyperlens magnifying sub-diffraction-limited objects. *Science* **315**, 1686 (2007).
14. Hoffman, A. J. *et al.* Negative refraction in semiconductor metamaterials. *Nat. Mater.* **6**, 946–950 (2007).
15. Scalora, M. *et al.* Negative refraction and sub-wavelength focusing in the visible range using transparent metallo-dielectric stacks." *Opt. Exp.* **15**, 508–523 (2007).
16. Smith, D. R., Kolinko, P. & Schurig, D. Negative refraction in indefinite media. *J. Opt. Soc. Am. B* **21**, 1032–1043 (2004).
17. Guo, Y., Cortes, C. L., Molesky, S. & Jacob, Z. Broadband super-planckian thermal emission from hyperbolic metamaterials. *Appl. Phys. Lett.* **101**, 131106 (2012).
18. Kabashin, A. V. *et al.* Plasmonic nanorod metamaterials for biosensing. *Nat. Mater.* **8**, 867–871 (2009).
19. Artigas, D. & Torner, L. Dyakonov surface waves in photonic metamaterials. *Phys. Rev. Lett.* **94**, 013901 (2005).
20. Lodahl, P. *et al.* Controlling the dynamics of spontaneous emission from quantum dots by photonic crystals. *Nature* **430**, 654–657 (2004).
21. Lounis, B. & Orrit, M. Single-photon sources. *Rep. Prog. Phys.* **68**, 1129–1179 (2005).
22. Hughes, S. Enhanced single-photon emission from quantum dots in photonic crystal waveguides and nanocavities. *Opt. Lett.* **29**, 2659–2661 (2004).
23. Lu, D., Kan, J. J., Fullerton, E. E. & Liu, Z. Enhancing spontaneous emission rates of molecules using nanopatterned multilayer hyperbolic metamaterials. *Nat. Nanotech.* **9**, 48–53 (2014).
24. Ferrari, L., Lu, D., Lepage, D. & Liu, Z. Enhanced spontaneous emission inside hyperbolic metamaterials. *Opt. Exp.* **22**, 4301–4306 (2014).
25. Sreekanth, K. V., De Luca, A. & Strangi, G. Experimental demonstration of surface and bulk plasmon polaritons in hypergratings. *Sci. Rep.* **3**, 3291 (2013).
26. Maas, R., Parsons, J., Engheta, N. & Polman, A. Experimental realization of an epsilon-near-zero metamaterial at visible wavelengths. *Nat. Photon.* **7**, 907 (2013).
27. Sreekanth, K. V., De Luca, A. & Strangi, G. Negative refraction in graphene-based hyperbolic metamaterials. *Appl. Phys. Lett.* **103**, 023107 (2013).
28. Yan, W., Shen, L., Ran, L. & Kong, J. A. Surface modes at the interfaces between isotropic media and indefinite media. *J. Opt. Soc. Am. A* **24**, 530–535 (2007).
29. Noginov, M. A. *et al.* Stimulated emission of surface plasmon polaritons. *Phys. Rev. Lett.* **101**, 226806 (2008).
30. Noginov, M. A. *Solis-sate random lasers*. New York: Springer (2005).
31. Ford, G. W. & Weber, W. H. Electromagnetic interactions of molecules with metal surfaces. *Phys. Rep.* **105**, 227403 (1984).
32. Cotter, N. P. K., Preist, T. W. & Sambles, J. R. Scattering-matrix approach to multilayer diffraction. *J. Opt. Soc. Am. A* **12**, 1097–1103 (1995).
33. Anttu, N. & Xu, H. Q. Scattering matrix method for optical excitation of surface plasmons in metal films with periodic arrays of subwavelength holes. *Phys. Rev. B* **83**, 165431 (2011).
34. Sreekanth, K. V., Zeng, S., Shang, J., Yong, K.-T. & Yu, T. Excitation of surface electromagnetic waves in a graphene-based Bragg grating. *Sci. Rep.* **2**, 737 (2012).
35. Husakou, A. & Herrmann, J. Steplike transmission of light through a metal-dielectric multilayer structure due to an intensity-dependent sign of the effective dielectric constant. *Phys. Rev. Lett.* **99**, 127402 (2007).
36. Palik, E. D. *Handbook of optical constants of solids*. Orlando, FL: Academic (1985).
37. Drake, J. M., Lesiecki, M. L., Sansregret, J. & Thomas, W. R. L. Organic dyes in PMMA in a planar luminescent solar collector: a performance evaluation. *Appl. Opt.* **21**, 2945 (1982).
38. Bouillard, J. S., Vilain, S., Dickson, W., Wurtz, G. A. & Zayats, A. V. Broadband and broadangle SPP antennas based on plasmonic crystals with linear chirp. *Sci. Rep.* **2**, 829 (2012).
39. Bartoli, F. J. & Gan, Q. Surface dispersion engineering of planar plasmonic chirped grating for complete visible rainbow trapping. *Appl. Phys. Lett.* **98**, 251103 (2011).
40. Zeng, S., Baillargeat, D., Hod, H. P. & Yong, K. T. Nanomaterials enhanced surface plasmon resonance for biological and chemical sensing applications. *Chem. Soc. Rev.* **43**, 3426–3452 (2014).
41. Stiles, P. L., Dieringer, J. A., Shah, N. C. & Van Duyne, R. P. Surface-Enhanced Raman Spectroscopy. *Annu. Rev. Anal. Chem.* **1**, 601–626 (2008).

Acknowledgments

We acknowledge support of the Ohio Third Frontier Project "Research Cluster on Surfaces in Advanced Materials (RC-SAM) at Case Western Reserve University".

Author contributions

K.V.S. and G.S. conceived the idea and designed the research. K.V.S. fabricated and characterized the samples, carried out ellipsometry and ultrafast optical experiments, and performed simulations and numerical modeling, and wrote the manuscript. K.H.K. fabricated the samples and performed the experiments. K.V.S., A.D.L. and G.S. analyzed the data. All authors discussed the results and commended on the manuscript.

Additional information

Supplementary information accompanies this paper at http://www.nature.com/scientificreports

Competing financial interests: The authors declare no competing financial interests.

How to cite this article: Sreekanth, K.V., Krishna, K.H., De Luca, A. & Strangi, G. Large spontaneous emission rate enhancement in grating coupled hyperbolic metamaterials. *Sci. Rep.* **4**, 6340; DOI:10.1038/srep06340 (2014).